AD-A082 634 TENNESSEE UNIV SPACE INST TULLAHOMA F/G 20/4
FLOW VISUALIZATION STUDY OF SECONDARY FLOW IN A CORNER.(U)
DEC 79 F G COLLINS AFOSR-78-3637
UNCLASSIFIED AFOSR-TR-80-0257 NL

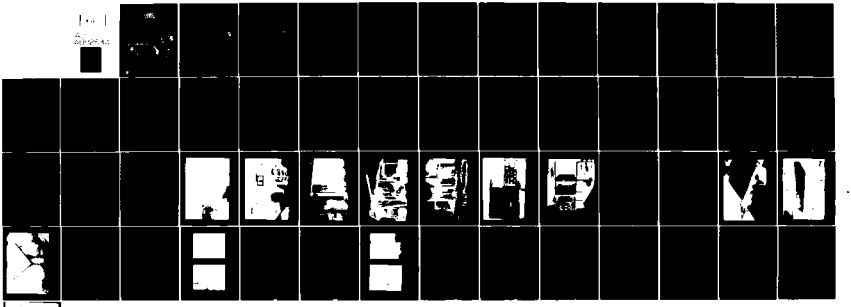

END
DATE FILMED
5-80
DTIC

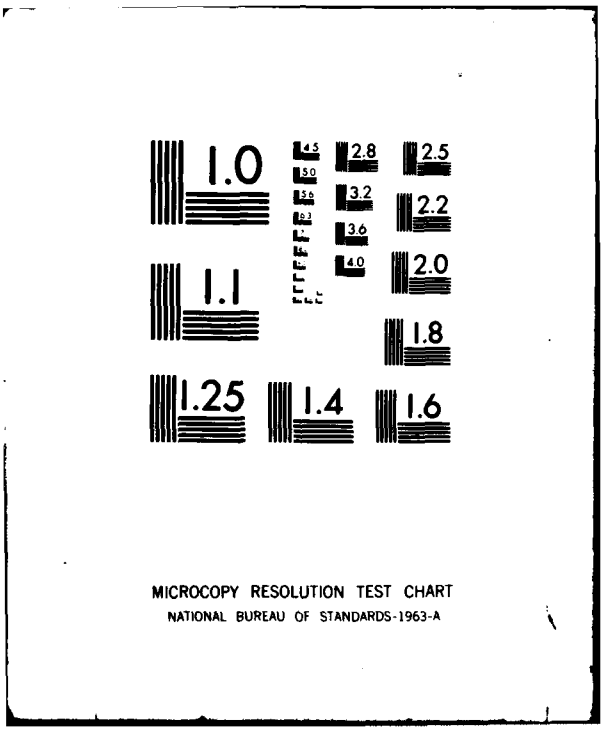
1.0
1.1
1.25
1.4
1.6
1.8
2.0
2.2
2.5
2.8
3.2
3.6
4.0
4.5
5.0
5.6
6.3
MICROCOPY RESOLUTION TEST CHART
NATIONAL BUREAU OF STANDARDS-1963-A

AFOSR-TR- 80-0257

LEVEL II

10

AD A082634

FLOW VISUALIZATION STUDY OF SECONDARY FLOW IN A CORNER

BY

FRANK G. COLLINS

DECEMBER, 1979

FINAL

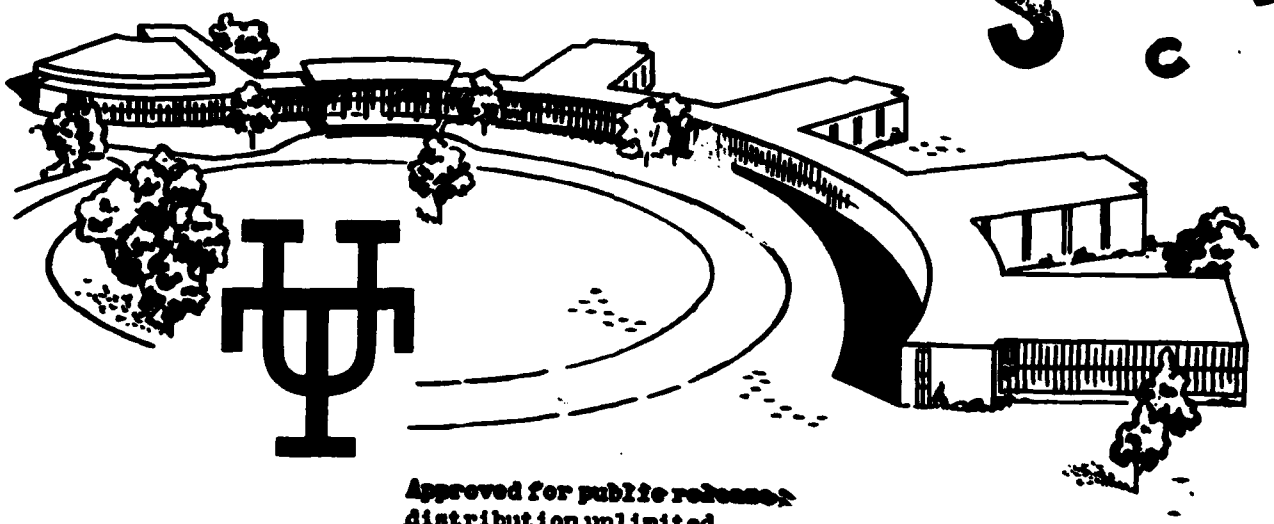

THE UNIVERSITY of TENNESSEE
SPACE INSTITUTE

Tullahoma, Tennessee

80 3 26 045

10

FLOW VISUALIZATION STUDY OF SECONDARY FLOW IN A CORNER

BY

FRANK G. COLLINS

DECEMBER, 1979

FINAL

Grant AFOSR-78-3537

Research Sponsored By

Air Force Office of Scientific Research

United States Air Force

Bolling A.F.B., D.C.

UNCLASSIFIED

SECURITY CLASSIFICATION OF THIS PAGE (When Data Entered)

REPORT DOCUMENTATION PAGE	READ INSTRUCTIONS BEFORE COMPLETING FORM
1. REPORT NUMBER: AFOSR-TR-80-0257	2. GOVT ACCESSION NO. / 3. RECIPIENT'S CATALOG NUMBER
4. TITLE (and Subtitle): FLOW VISUALIZATION STUDY OF SECONDARY FLOW IN A CORNER	5. TYPE OF REPORT & PERIOD COVERED: FINAL rept. 01 Jan 78 - 30 Jun 79 / 6. PERFORMING ORG. REPORT NUMBER
7. AUTHOR(s): FRANK G. COLLINS	8. CONTRACT OR GRANT NUMBER(s): AFOSR-78-3537
9. PERFORMING ORGANIZATION NAME AND ADDRESS: THE UNIVERSITY OF TENNESSEE SPACE INSTITUTE, TULLAHOMA, TN 37388	10. PROGRAM ELEMENT, PROJECT, TASK AREA & WORK UNIT NUMBERS: 2307A4, 61102F
11. CONTROLLING OFFICE NAME AND ADDRESS: AIR FORCE OFFICE OF SCIENTIFIC RESEARCH/NA, BLDG 410, BOLLING AFB DC 20334	12. REPORT DATE: Dec 79 / 13. NUMBER OF PAGES: 49
14. MONITORING AGENCY NAME & ADDRESS (if different from Controlling Office)	15. SECURITY CLASS. (of this report): UNCLASSIFIED / 15a. DECLASSIFICATION/DOWNGRADING SCHEDULE

16. DISTRIBUTION STATEMENT (of this Report)

Approved for public release; distribution unlimited.

17. DISTRIBUTION STATEMENT (of the abstract entered in Block 20, if different from Report)

18. SUPPLEMENTARY NOTES

19. KEY WORDS (Continue on reverse side if necessary and identify by block number)

CORNER FLOW
SECONDARY FLOW
FLOW VISUALIZATION
VORTEX FORMATION

20. ABSTRACT (Continue on reverse side if necessary and identify by block number)

An experimental investigation has been made of secondary flow in a 90 degree corner. The tests were run in a water tunnel at low speed (approximately 0.3 ft. per sec.) with emphasis on an attempt to visualize the embedded vortices in the laminar flow. The Reynolds number range was 11,000 to 52,500 per foot; the corner model was 9.75 in. wide by 48 in. long. The model was aligned in the tunnel so that no streamwise pressure gradient was present. Flow visualization was by means of hydrogen bubbles and dye. None of the

DD FORM 1 JAN 73 1473 EDITION OF 1 NOV 65 IS OBSOLETE

UNCLASSIFIED 387070

streak-lines examined with either the bubbles or the dye showed any indication of the presence of secondary motion in the first 18 inches of the corner. This is not believed to be conclusive since the vortices may exist at other distances along the corner (the limit here was imposed by the flow visualization apparatus used) or may be poorly developed in the initial length examined.

TABLE OF CONTENTS

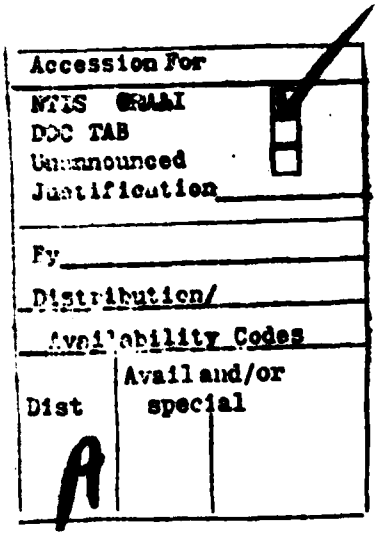

I. INTRODUCTION

Today there is great interest in designing military and commercial aircraft of minimum drag, both to improve performance and to save fuel (Ref. 1). To adequately compare competing designs it is important that the drag of the aircraft be accurately predicted from the wind tunnel tests. A drag prediction accuracy of one drag count is presently required.

The drag coefficient measured for a model of the flight vehicle must be extrapolated to the flight Reynolds number. Aircraft companies presently go through a complicated drag prediction process which includes not only the Reynolds number extrapolation but also the addition of drag increases due to roughness, engine interference, appendages, etc. (Ref. 2 to 6).

The Reynolds number extrapolation procedures must be very accurate because the corrections are large (up to 20% - see Ref. 5), and errors in their magnitude will invalidate the comparison between the projected and measured vehicle performance. The extrapolation procedures used are validated by comparing with previous tunnel/flight test correlations on geometrically similar vehicles. Therefore, new designs are frequently only incrementally different from previous ones where the tunnel/flight correlation is well known.

Several flow features are presently corrected for the flight Reynolds number, including the location of the boundary layer transition and skin friction drag. These procedures,

however, are at best semi-empirical. Of greater concern, though, is the interference between various parts of the aircraft, including the wing-body junction, engine-airframe integration, pylon-store-wing interference, winglet-wing junction, etc. At higher transonic and supersonic Mach numbers these interferences lead to strong viscous-inviscid interactions (Ref. 7) while at lower Mach numbers the interactions are strongly viscous. They may lead to flow separation (Ref. 8) and must be geometrically modeled accurately on the wind tunnel model because the measured drag is sensitive to geometry (Ref. 9 and 10).

Three-dimensional flow interactions are also one of the major reasons that many aircraft do not meet the desired performance during the first flight tests. According to Hagerman (Ref. 11) eighty-five percent of the tunnel tests performed on aircraft which had encountered problems during flight test uncovered interference problems with the original design. Tests designed to correct the interference problems have been performed in low speed tunnels or water tunnels using flow visualization diagnostic techniques. Such a procedure was used to reduce the drag coefficient of the C-5A (before flight test) by 57 drag counts by indicating geometrical changes of the wing-fuselage junction and the wheel housing that would reduce the separation found on the original configuration. A wax model was used so that fast geometrical changes could be made (Ref. 10). More use of low speed tunnels and water tun-

nels will be made in the future to identify and correct interference problems at an early stage in the design cycle (Ref. 11). The technique has been very successful for improving the performance of transonic transport aircraft.

The drag coefficient extrapolation procedures are not very accurate and do not meet the requirement for an accuracy of one drag count. Improved extrapolation procedures will require, among other things, an increased understanding of the interaction phenomena which occur at such locations as the wing-fuselage junction.

The flow interactions result in regions of boundary layer separation, in secondary flows, in complex three-dimensional vortical fields, and in surfaces of high shear. At supersonic Mach numbers these flow features lead to practical problems which influence aircraft performance including loss of control effectiveness, flow degradation at an engine inlet, and high heating rates where a shear layer reattaches to the body (Ref. 7). In subsonic and transonic flow they lead, in addition, to an increased drag. In general, the flow patterns which are generated by the viscous interactions are among the most complex that exist but their importance demands that they be understood.

In the future the computer will make a continuously increasing contribution to the aircraft design process as more computational techniques are validated and computer speeds and

sizes are increased (see summary in the report of the 1977 AFOSR/ASEE Summer Design Study Program, Ref. 12). Computations will make a significant contribution by allowing more design by analysis and thereby will help eliminate the reliance upon experience obtained from previous tunnel and flight tests on geometrically similar vehicles. However, computations will not be able to handle all geometries in the foreseeable future and some important design aspects, such as the complicated three-dimensional wing-fuselage interaction flow, will continue to be examined in the tunnel (Ref. 5).

The types of problems that can be computed with no empiricism in the near future depend upon whether a suitable turbulence model will be available or not (Ref. 12). Assuming the existence of a satisfactory turbulence model, three-dimensional viscous flows which are dominated by the external pressure gradient (such as cross flows over fuselages) will be computable, but those flows which are primarily viscous interactions (e.g., wing-body junction with embedded secondary vortices) will not be. The embedded vortices will have to be added empirically. This will mean that while many individual aircraft components can be analyzed by computations the interactions between the individual parts will still have to be measured in the tunnel.

The present study is an experimental investigation of the secondary flow in a 90° corner at low speeds. This configuration is related to the flow in the wing-fuselage inter-

section, for example. Not only will the results of this investigation assist in the aircraft design process and drag extrapolation but there is more general interest in this type of flow. As new computational techniques become available for application to aircraft design it will be necessary to validate them by comparing computations with experimental measurements of some geometrically simple flows. The corner flow offers such a possibility. Marvin, of NASA Ames (Ref. 13 and 14), lists the corner flow as one of the compressible three-dimensional bench mark experiments to be used in the creation of accurate numerical techniques that are applicable to the nonlinear Navier Stokes equations.

The configuration examined has the following features that make it ideal as a benchmark experiment:

- Simple geometry with three-dimensional flow (embedded vortices);
- Laminar flow so that a comparison of experiments with numerical computations can separate numerical errors from turbulence modeling errors;
- A boundary region flow so the usual boundary layer approximations cannot be used to affect much simplification of the Navier Stokes equations;
- Incompressible flow with constant fluid properties;
- Zero pressure gradient;
- Steady flow in the mean;
- Zero skin friction in the corner, leading to a separation velocity profile.

The experiments were performed in a water tunnel with low free stream velocities (less than 0.3 ft./sec.). The emphasis was on attempting to visualize the embedded vortices for laminar flow. Previous investigations had failed to visually locate the vortices because of the experimental problems involved (Ref. 15). However, indirect evidence had indicated the presence of vortices which were rotating oppositely to those for turbulent flow.

Previous theoretical and experimental work on the corner flow problem is examined in Section II. Section III describes the new UTSI water tunnel while the corner flow model that was used is described in Section IV. Part II of the report will discuss the results and conclusions of the experimental program and give recommendations for future experiments.

II. CORNER FLOW

The general Navier Stokes equations for a three-dimensional flow are very complicated, even for incompressible, steady, laminar, constant property flows. Therefore, it is important to attempt to simplify the equations. In the following discussion the coordinate x will be assumed to be in the direction of the external stream.

Three-dimensional flow fields have been placed in three classes (ref. 16 and 17). They are:

a) "Thin shear layers" for which the following approximations is valid

$$\frac{\partial}{\partial y} >> \frac{\partial}{\partial x} \sim \frac{\partial}{\partial z} \quad ;$$

b) "Slender shear flows" or "boundary region flows" where

$$\frac{\partial}{\partial y} \sim \frac{\partial}{\partial z} >> \frac{\partial}{\partial x} \quad ;$$

c) "Fully three-dimensional flow" for which

$$\frac{\partial}{\partial x} \sim \frac{\partial}{\partial y} \sim \frac{\partial}{\partial z} \quad .$$

The flow in a corner, which was examined in this work (Figure 1) is an example of a boundary region flow. Although the geometry is very simple the flow is not. Using the ordering given above it can be seen that the corner flow has a scale L in the x - direction but a scale δ, where $\delta << L$, in both the x & y directions.

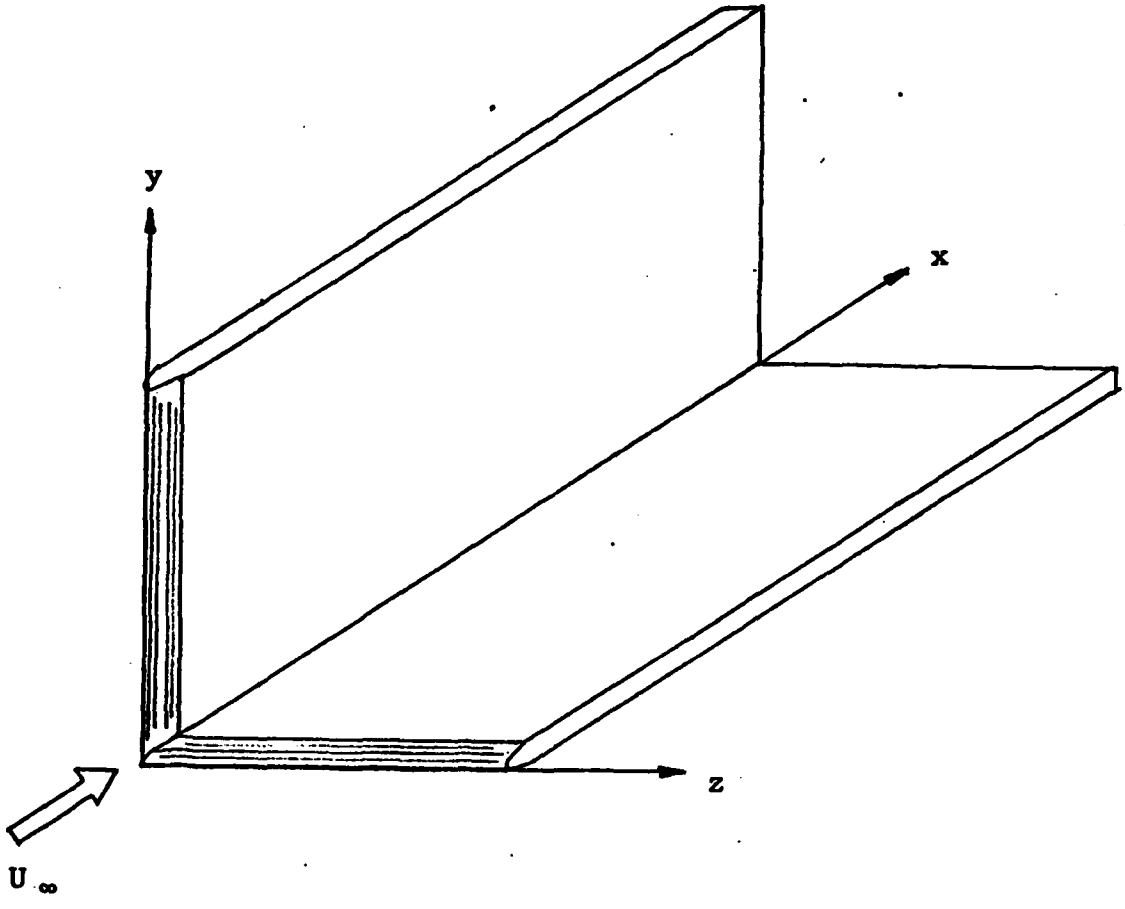

Fig. 1. Corner flow model.

Also, boundary region flows are characterized by large or irregularly varied lateral curvature where the thickness of the viscous layer is not small compared to the lateral radius of curvature of the surface.

Consider only geometries with curvatures lateral to the stream direction (in y - z plane) but not in the stream direction. Assume that there is no streamwise pressure gradient. By applying the appropriate ordering of the magnitude of the terms for the boundary region flow in the continuity and momentum equations it can be shown that only the components of the stress gradients in the stream (x) direction can be neglected (ref. 17). All four equations are required to describe the flow and the resulting equations are elliptic rather than parabolic, in contrast to the boundary layer equations (ref. 18). Therefore, downstream influences can have an important effect upon the flow. The effect of the lateral curvature is contained in some of the remaining viscous terms. It can be shown that extreme lateral curvature destroys the boundary layer similarity and the velocity profile in the boundary region continuously changes its shape as the flow proceeds along the generators away from the leading edge.

The corner flow problem where two walls intersect abruptly at 90° (the problem studied) has received comparatively little attention because of the mathematical difficulties involved. No unique normal direction exists at a boundary layer point close to the corner and hence lateral diffusion must be reinstated to the normal boundary layer equations. Usually the pressure is

eliminated from the system of equations in favor of the equation for the streamwise component of vorticity. The generation of streamwise vorticity is a major new feature of three-dimensional flows. If the vorticity components in the x, y, z - directions are indicated by ξ, η, ζ, respectively, the equation for the rate of change of streamwise vorticity, using the boundary region approximation (ref. 17), is

$$\frac{D\xi}{Dt} = \xi \frac{\partial u}{\partial x} - \frac{\partial u}{\partial y}\frac{\partial w}{\partial x} + \frac{\partial u}{\partial z}\frac{\partial v}{\partial x} + \nu \left(\frac{\partial^2}{\partial y^2} + \frac{\partial^2}{\partial z^2}\right) \xi \quad .$$

In laminar flow this equation represents the net effect of viscous diffusion of vorticity and of the stretching and skewing of vorticity by the components of the rate of strain. In nearly parallel flow, such as shown in Figure 1, ξ will be much less than η and ζ.

Theoretically the skin friction is zero at an abrupt corner since the velocity gradients in the lateral directions along the corner plate are both zero. Thus the laminar corner layer profile should be of the separating type.

Indirect experimental evidence indicates the presence of secondary flows in the corner for both laminar (ref. 19) and turbulent flow (ref. 20 to 23), although the mechanism for their creation is thought to be quite different. Secondary motions are driven by four principle mechanisms (ref. 16), namely:

1. Lateral (spanwise) convergence or divergence of the velocity components of potential flow parallel to the wall. This

mechanism influences the boundary layer thickness and profile and the wall shear stress. Collateral velocity vectors exist through the boundary layer.

2. Lateral curvature of the potential flow which leads to skewed velocity profiles through the boundary layer.

3. Lateral wall motion of a bounding surface relative to the fluid. Viscous drag then leads to secondary motions.

4. Gradients of the Reynolds stresses can lead to forces in the secondary flow plane which induce secondary velocities. Mechanisms 2 and 3 were called secondary motion of the first kind by Prandtl and mechanism 4 was called secondary motion of the second kind.

The last mechanism is the only one that can create secondary flows in a straight corner region such as that shown in Figure 1. However, in laminar flow none of the above mechanisms are applicable. In laminar flow the secondary motion is thought to be associated with the progressive changes in the form of the velocity profiles (ref. 19) or to be the result of a localized instability in the corner, where the velocity profiles have points of inflection (ref. 24). Presently it is not possible to predict the presence of these embedded vortices from theory, even for laminar flow, and they must be added empirically (ref. 25).

The earliest measurements of flows in corners were those performed for turbulent flows in ducts of various non-circular cross sectional shapes. Some of this early work is summarized by Schlichting (ref. 26 - also see ref. 21). Nikuradse made

the earliest measurements of the isotach lines (lines of constant velocity in a plane normal to the mean flow direction) in rectangular ducts and Prandtl speculated that their peculiar shape near the corner was due to the presence of secondary motions. It is also reported that Nikurdse made visual observations of the secondary flows. Prandtl and others then put forth theoretical explanations for the existence of the secondary motions which involved the form of the turbulent structure of the flow. Because the early theories involved the turbulent structure of the flow it was thought that secondary motions did not occur for laminar flow. A schematic of the secondary motion for turbulent flow in a rectangular channel is shown in Figure 2.

Just as most of the measurements in ducts were made with turbulent flow likewise most of the corner flow measurements were made with turbulent flow (ref. 20, 21, and 22). Most of the evidence for secondary motion in the corner is indirect, because flow visualization has not been used, but Gessner and Jones measured the secondary motion patterns using a hot wire (ref. 22). A typical secondary motion and associated isotach is shown schematically in Figure 3 for turbulent flow. As mentioned previously, the creation mechanism for the secondary motion for laminar flow is quite different from that for turbulent flow and it was long thought that it did not even exist. The measurements of Zamir and Young (ref. 19), however, show its presence but in a rotational sense opposite to that for turbulent flow (see Figure 3b). They inferred the presence of secondary motion from the shape of the

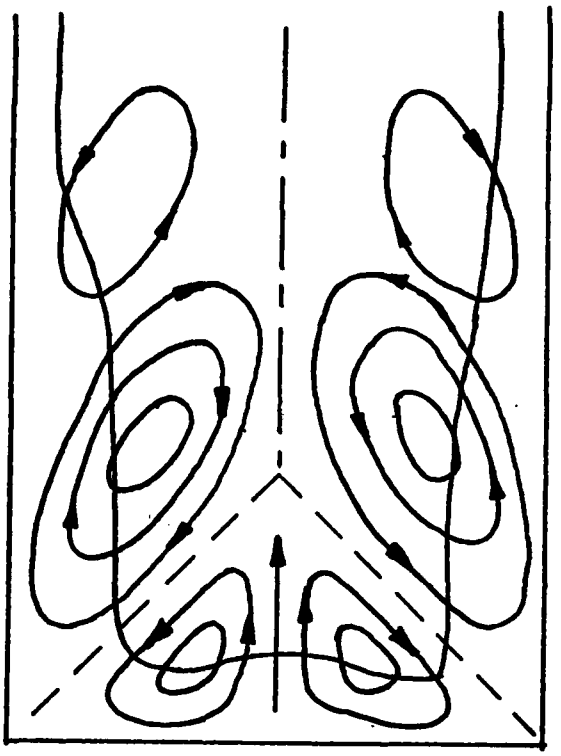

Fig. 2. Secondary motion and isotach in a rectangular pipe (ref. 26).

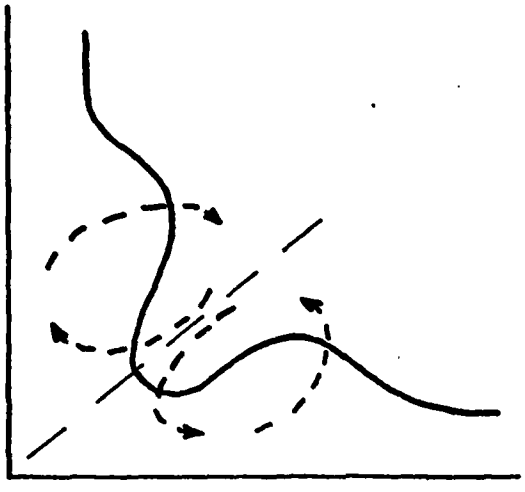

(a) Secondary motions and isotach for turbulent flow (ref. 20 and 21).

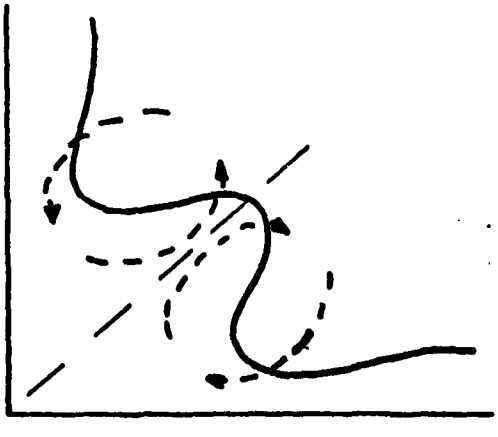

(b) Secondary motion and isotach for laminar flow (ref. 19)

Fig. 3. Corner flow secondary motion.

isotachs and from surface visualization. The secondary motion was thought to be associated with progressive changes in the form of the velocity profiles and was found to be more pronounced than for turbulent flow.

Their measurements confirmed the speculation that the skin friction was zero (or at least very small) at the corner and that the velocity profile changed progressively from the Blasius profile to a separating profile, with an inflection point, as the corner was approached. Transition began at $Re_x = 6 \times 10^4$ and turbulent spots appeared at $Re_x = 2 \times 10^5$. The progressive changes in the velocity profiles were very pronounced prior to transition and may have been linked to the transition process.

The transition process was found to be different from that on a flat plate because regular waves appeared before the appearance of the turbulent spots. Transition appeared first near the corner and then spread laterally as the flow proceeded downstream. Even though the corner profile was of the separating type they found no evidnece of reverse flow. However, the flow violently spearated in the presence of an adverse pressure gradient.

Zamir and Young speculated that the secondary motions that they observed could have been the result of flow instability that occurs before transition takes place. Experiments performed at lower Reynolds numbers would be required to settle that question.

Theoretical work on the flow in a corner has been confined to laminar flow. The secondary motion does not result from a general solution but its existence must be assumed and it must be added. The first published treatment of this problem was by

Carrier (ref. 27). The solution was not correct, however, because the streamwise vorticity equation was not satisfied. Approximate techniques such as the momentum-integral method have been applied to the problem (see refs. 28 and 29) but they cannot give details of the flow structure. Mager (ref. 29) added a pair of streamwise vortices as shown in Figure 4.

Recent theoretical analysis of the laminar flow in the corner has used the method of matched asymptotic analysis to model the secondary motion. Streamwise vorticity was taken into account by Rubin (ref. 30) who partitioned the flow into four regions: the potential flow region, the boundary layer region, and the corner-flow region, plus regions of overlap. Numerical solutions (ref. 31) indicated swirling motion in the corner but no closed vortical patterns. However, the mean velocity profiles were not in agreement with measured results.

Tokuda (ref. 32) added another region in the corner which contained Stokes flow (Fig 5) and was able to explain the observed mean velocity profiles. The corner secondary motion was found to be very complex and numerical results were not given because of mathematical difficulties resulting from the nonlinear equations.

Additional recent work has been performed by Ghia, again using the method of matched asymptotic analysis plus numerical solutions (ref. 33 and 34). Turbulent corner flows are also discussed by Johnston (ref. 16).

The conclusion of this examination of previous investigations of the laminar corner flow is that very little is known about the

lw

secondary motion itself or of the role that transition plays in the existence of the secondary motion. Also, the reason why the rotational sense is different for laminar and turbulent motion and how it changes through the transition region is not known.

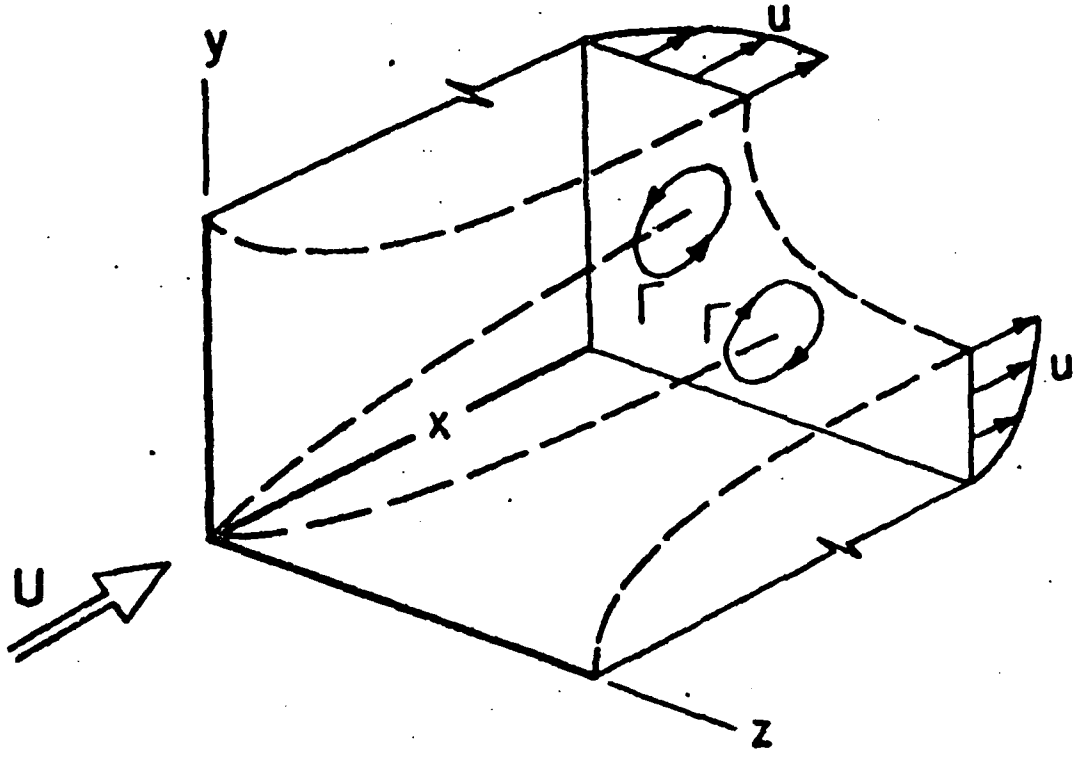

Figure 4. Corner flow problem examined by Carrier (Ref. 26) for laminar, incompressible flow.

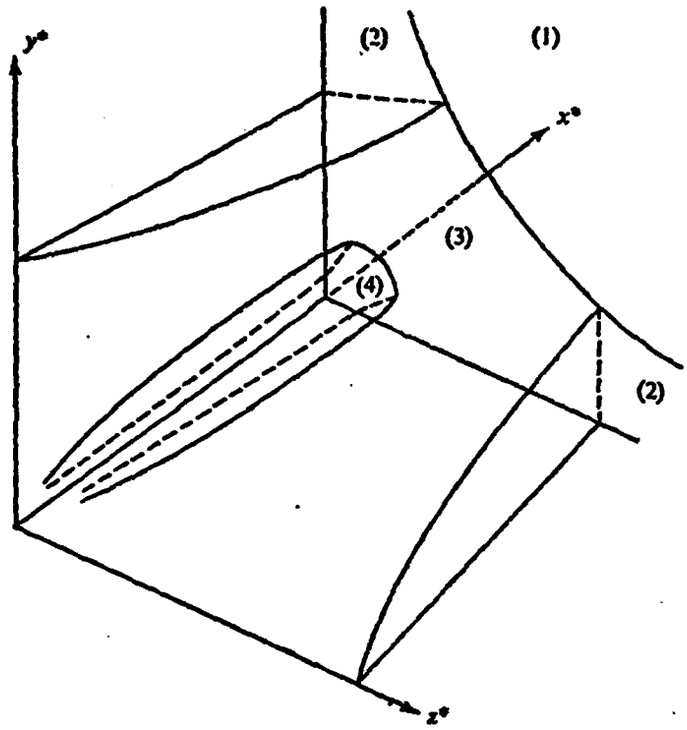

Fig. 5. Flow past a right-angle corner and the co-ordinate system. (1) Potential-flow region, (2) Boundary-layer region, (3) Corner-layer region, (4) Stokes region (Ref. 32).

III. WATER TUNNEL

The experiments were performed in the UTSI water tunnel. The water tunnel had been used previously for a number of jet and vortex studies but had been disassembled before the initiation of the present work. Advantage was taken during reassembly to add numerous improvements to the tunnel. Most of the effort during the research period was spent on the reassembly of the tunnel.

An overall diagram of the water tunnel is shown in Figure 6. The tunnel has a closed circuit and a closed test section. The test section is enclosed by a light tight building whose inside walls have been blackened for photographic purposes (Figures 7, 8, and 9). The tunnel is constructed from ¼ inch thick mild steel that is protected with Sherwin Williams Paint Company SHER-TAR black epoxy paint. Two expansion bellows are provided in the return pipe. The water volume is about 2100 gallons.

The test section is constructed of ½ inch thick plexiglas. The cross section is 12 inches by 18 inches and is 59 inches long. The method of Thwaites (Ref. 18, p. 303)was used to calculate the growth of the boundary layer on the nozzle and test section walls and the test section walls were diverged to account for the growth of the boundary layer at a free stream speed of 0.5 ft./sec. The model is supported on two linear motion feedthroughs attached to the lower wall of the

test section. The flow in the test section can be viewed from the four sides of the test section and from an end viewing port downstream of the test section (Figure 8).

The tunnel is powered by a propeller which is located at the second bend (Figures 6 and 9). A 10 inch diameter two-bladed propeller is connected by a shaft to a one horsepower motor. The motor is connected to a continuously variable speed transmission which allows the test section speed to be varied from 1 in./sec. to greater than 1 ft./sec. The fluctuations from the propeller are damped by the long return pipe (equivalent L/D = 75) (Figure 10). The motor is on vibration mounts and is flexibly connected to the propeller shaft.

The stilling chamber (Figures 10 and 11) is 61 inches in diameter and is 112 inches long. It contains four stainless steel screens and two aluminum honeycombs that were designed according to the work of Loehrke and Nagib (Ref. 35). The wire diameter of the largest screens (16 x 16 mech, 0.018 inch diameter wire) was chosen to keep the Reynolds number based on wire diameter and stilling chamber water speed less than 40. The turbulence generated by the largest screen was then allowed to decay by placing the honeycomb 500 wire diameters (9 inches) downstream of the first screen. A honeycomb was placed at that location (0.001" thick aluminum, ¼ inch cell diameter, 1½ inch thick, $\ell/d = 6$). The shear

layers leaving the honeycomb were broken up by placing a 40 x 40, 0.0065 inch diameter, screen immediately downstream of the honeycomb. The honeycomb was designed to have a turbulence level of 0.1% in the test section. For the given mesh size and contraction ratio this required a settling length of at least 16-3/4 inches. This series of screens and honeycomb was repeated again after a decay length downstream of the first honeycomb.

The nozzle was a bell mouth that continuously changed from a circular shape to a rectangular shape. It had a contraction ratio of 13.5. It was so designed that the boundary layer had a constant thickness along its surface.

While changing the model and during cold nights the water could not be stored in the tunnel. Therefore, a 4000 gallon underground storage tank was constructed (Figure 11). The water is then pumped back into the tunnel for use. The water is conditioned with sodium sulphate (2% by weight) to increase its electrical conductivity and 0.1% sodium dichromate to inhibit corrosion.

A small portion of the main flow is bypassed through a woven polypropylene cartridge filter to filter the water to 10 microns (100%) (Figures 6 and 8). A process glass pipe is placed on top of the stilling chamber (Figure 10) and pumped on by aspirator pumps (Figure 8) to degas the water. The glass pipe also allows the water in the test section to be overpressured by 2 psi which increases the quality of the

hydrogen bubble flow visualization.

The tunnel is controlled from a master control panel inside the building (Figure 12). All valves are solenoid operated. The tunnel speed is measured with a 5/16 inch diameter pitot-static tube that is placed upstream of the test section (Figure 7). A thermocouple measures the water temperature at the same location. A single-channel constant temperature anemometer is also available.

The dynamic pressures expected in the tunnel free stream are very small (7.4×10^{-4} psi at a test section velocity of 1/3 ft./sec.). To align the model and eliminate streamwise pressure gradients it is necessary to measure a pressure coefficient of 0.01 (Ref. 19). Therefore, differential pressures less than 10^{-5} psi need to be measured in the tunnel. A Gould Datametrics Type 590 integral Barocel differential pressure transducer with a Type 552 liquid medium isolator was purchased to measure these small pressure differences (Figure 13). The transducer has a full scale range of 0.193 psi with an accuracy of 0.01% FS, or 1.9×10^{-5} psi.

The hydrogen bubbles are generated from a 0.001 inch diameter platinum wire cathode (anode is connected to the model, further downstream). The wire is connected to a commercial dc power supply (Figure 13). The bubbles are only generated continuously.

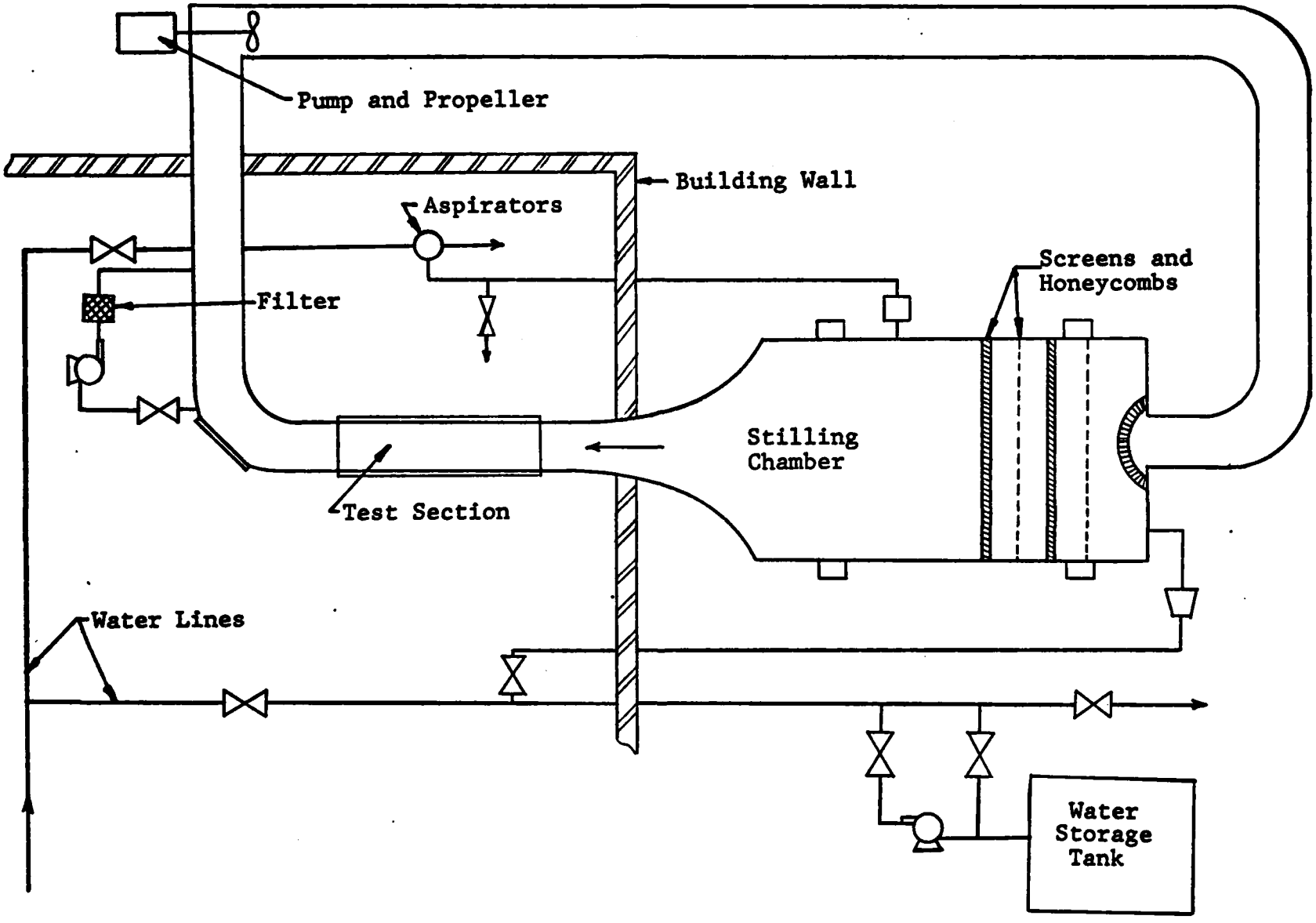

FIGURE 6 Diagram of UTSI Water Tunnel Facility

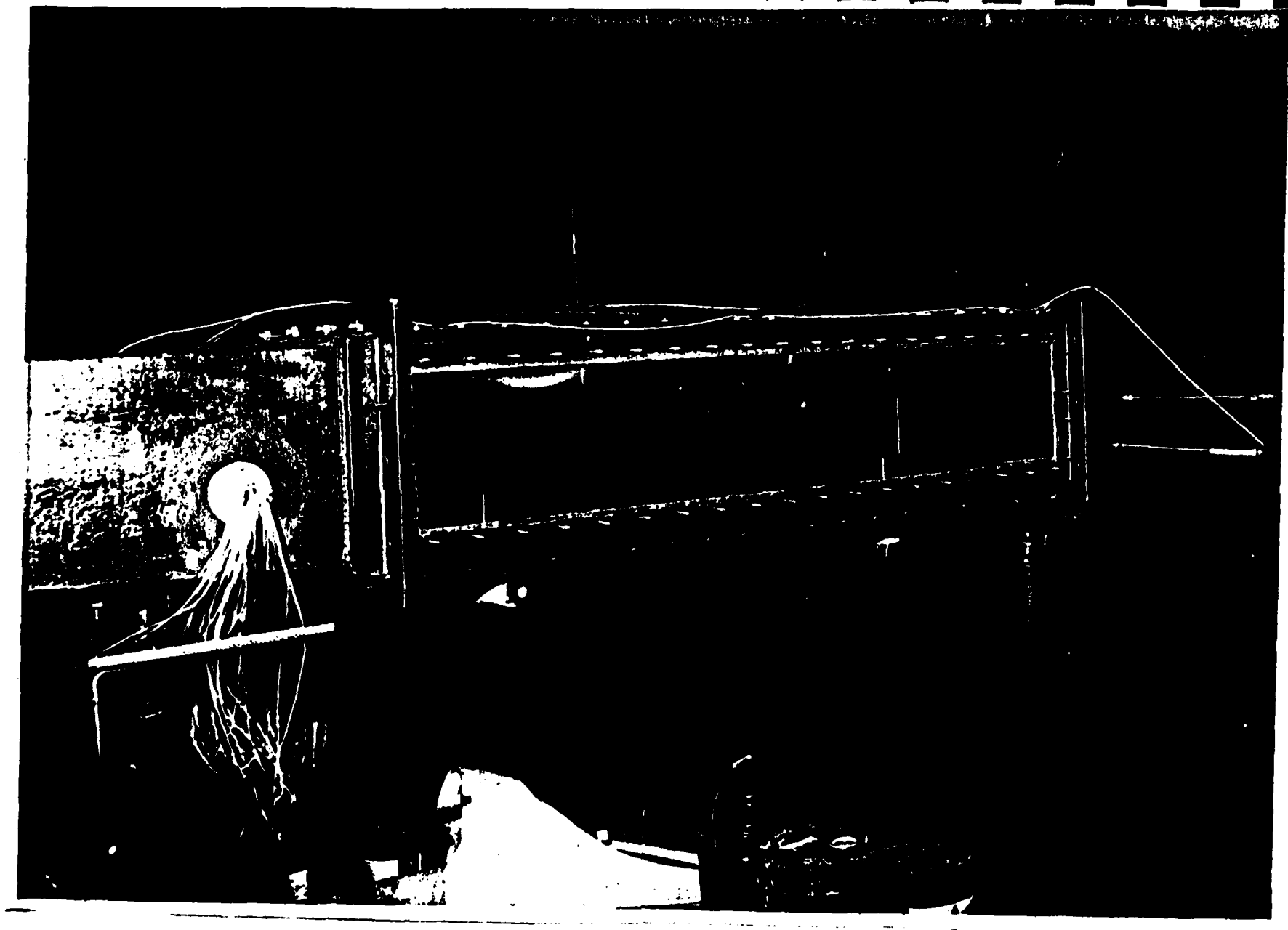

Figure 7 Test Section

Figure 8 Overall View of Water Tunnel

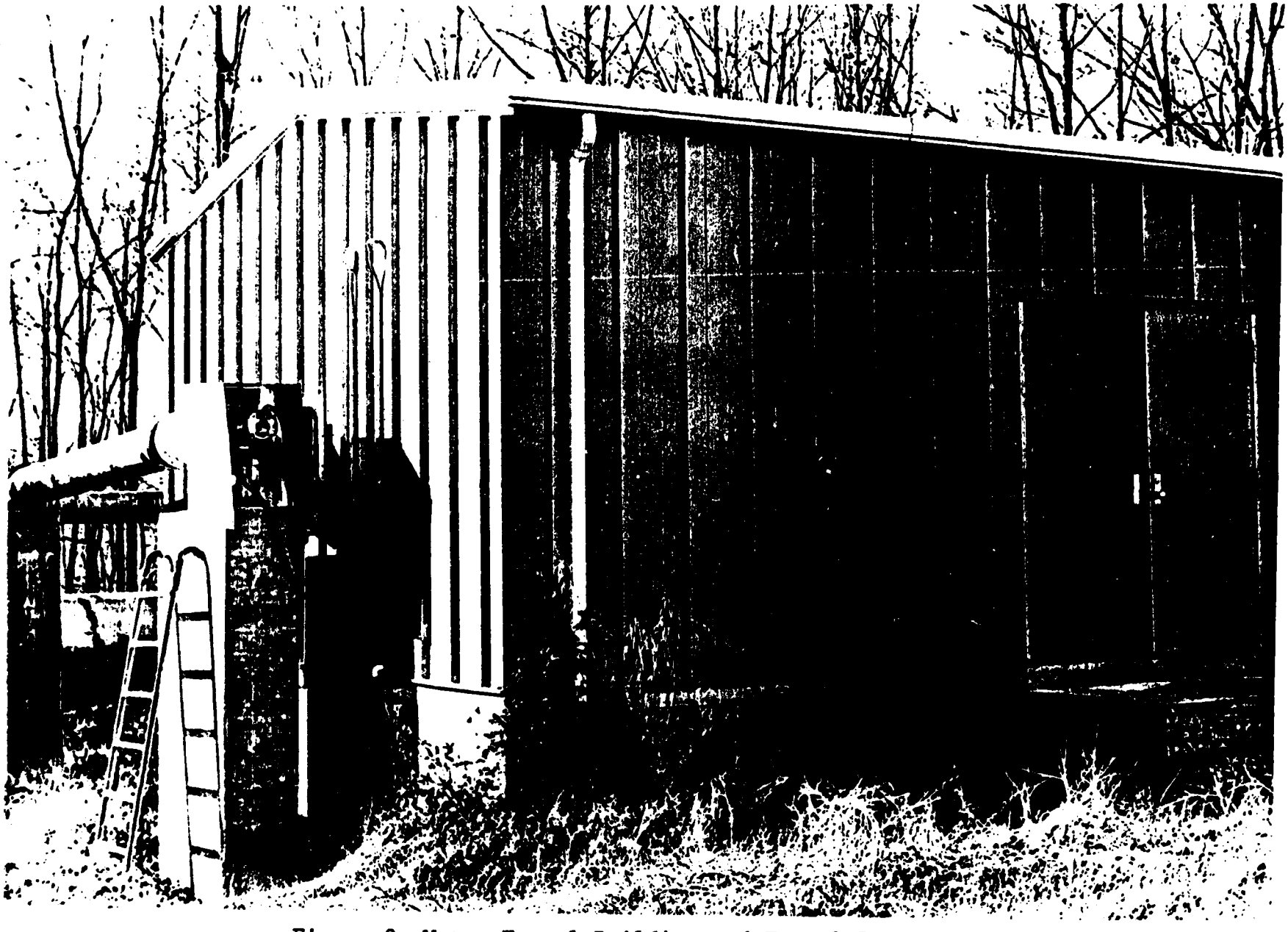

Figure 9 Water Tunnel Building and Tunnel Pump

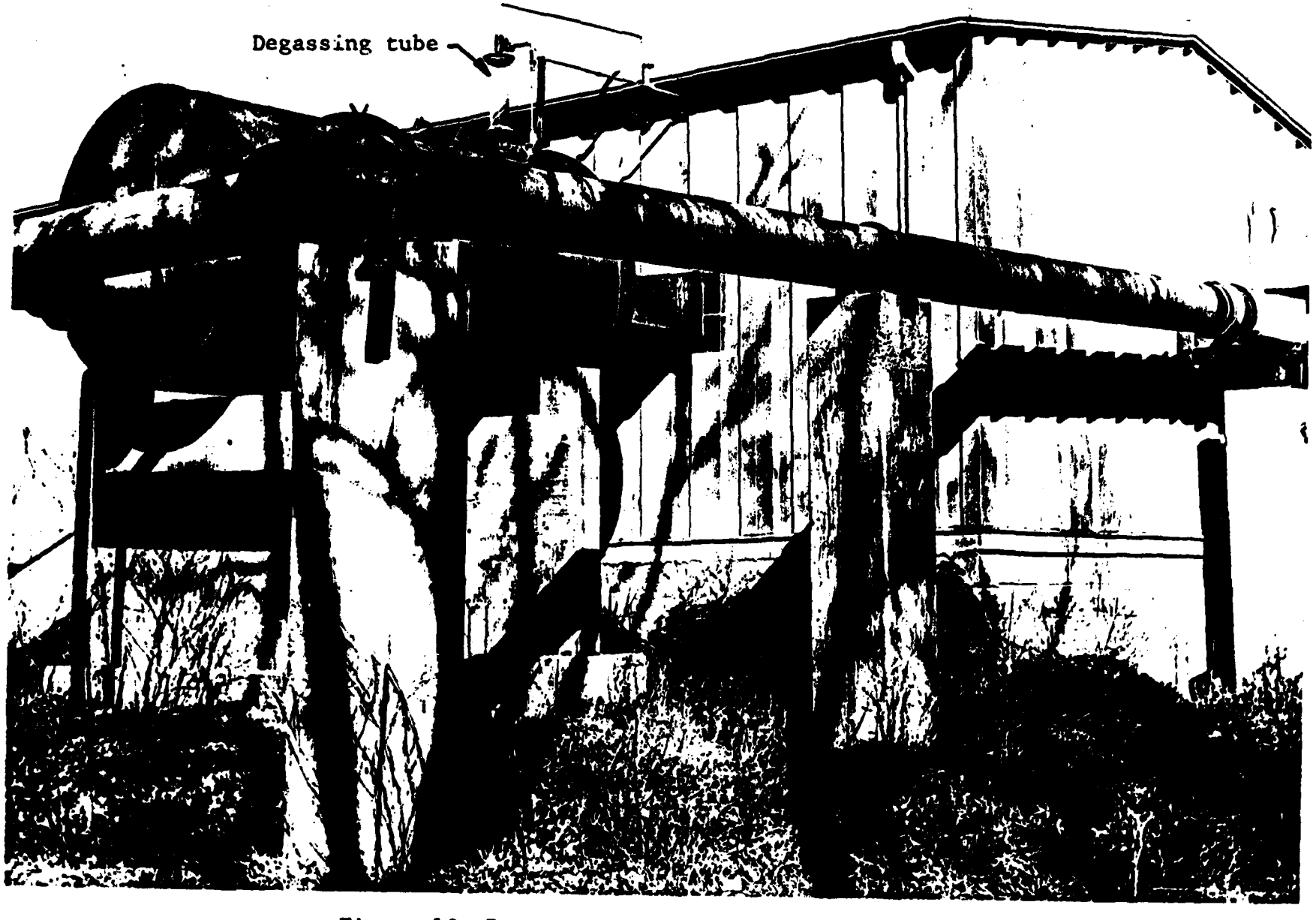

Figure 10 Return Pipe and Stilling Chamber

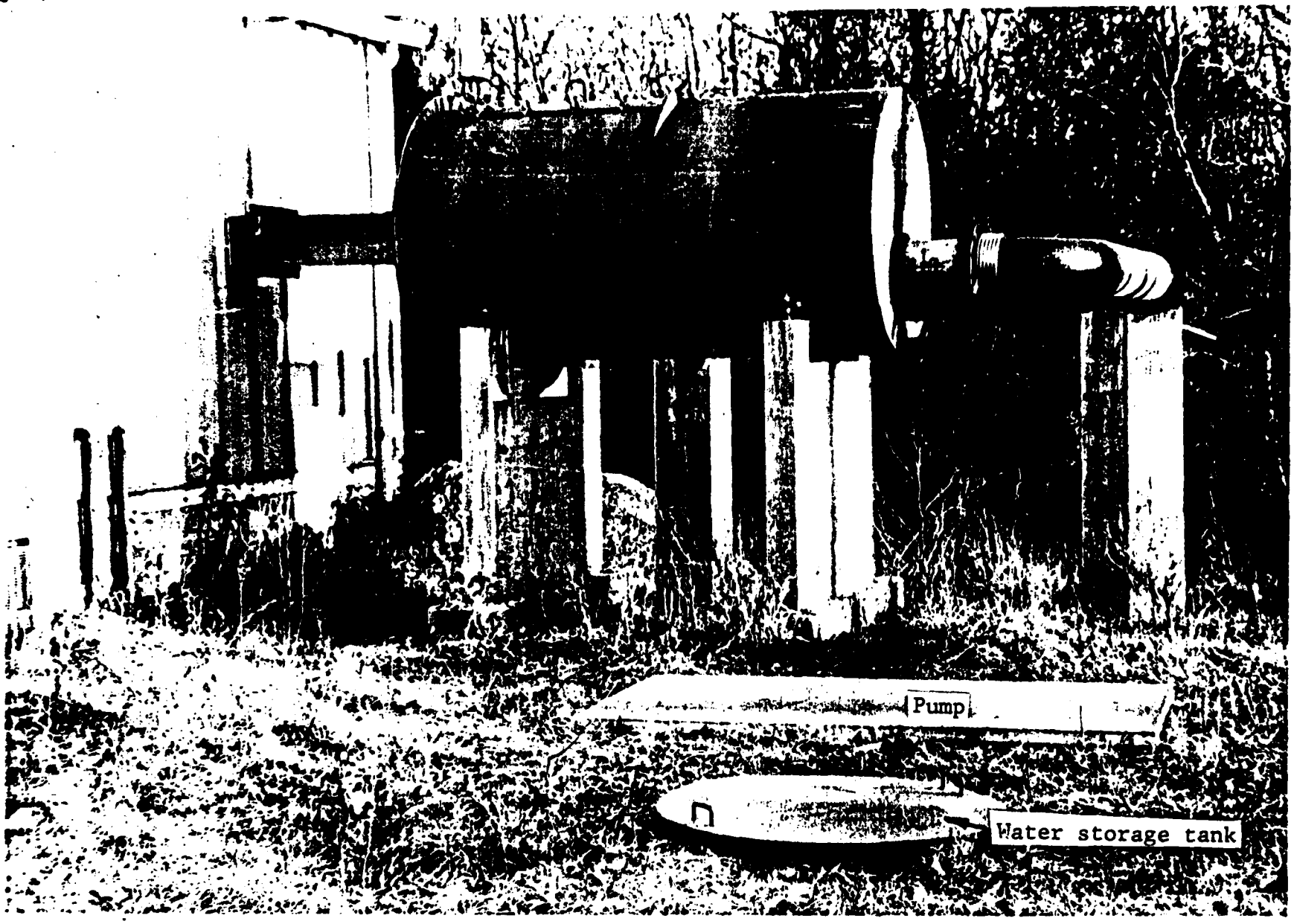

Figure 11 Water Storage Tank

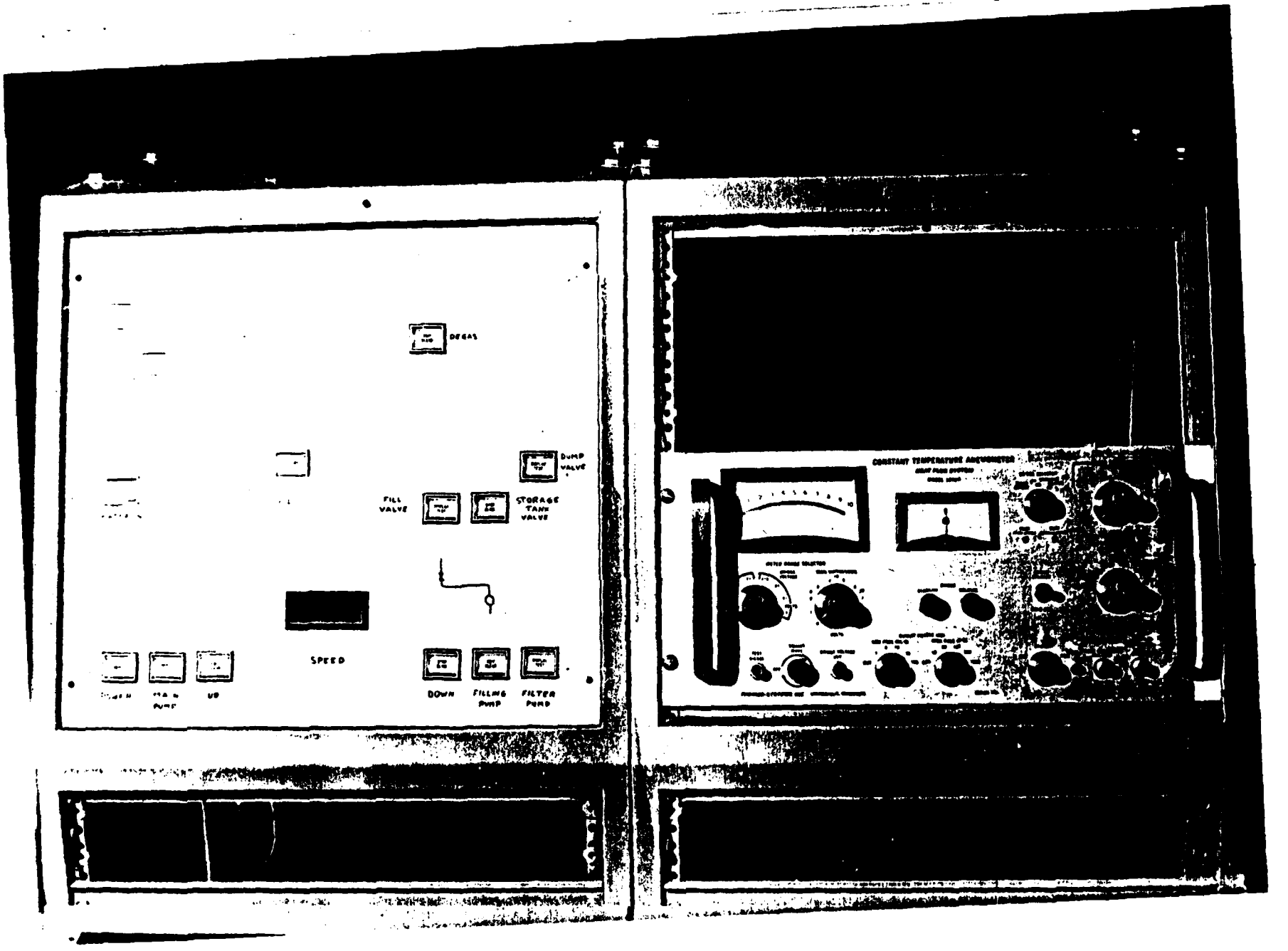

Figure 12 Tunnel Controls

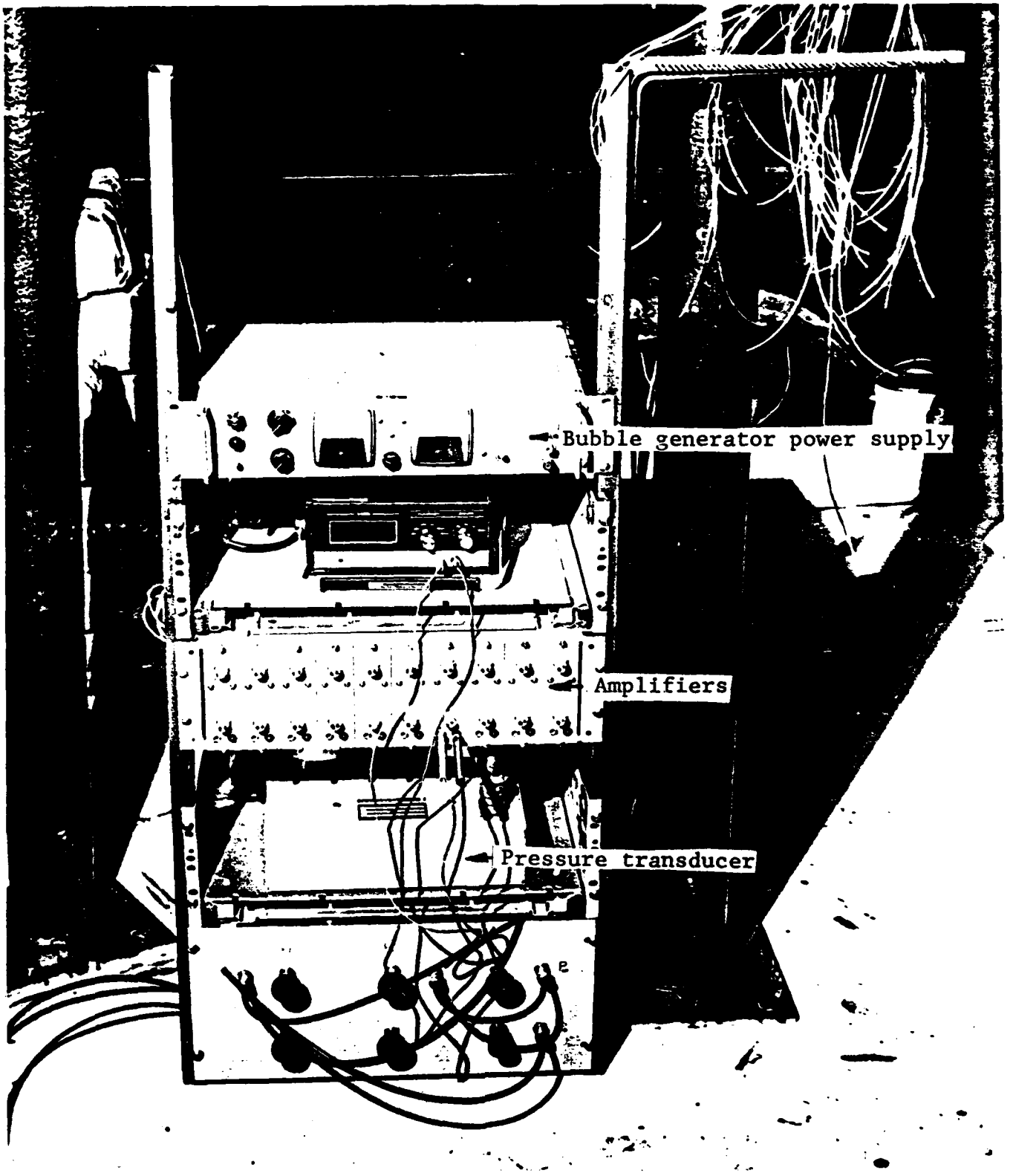

Figure 13 Electronics

IV. CORNER FLOW MODEL

The experiments were performed on a model consisting of two flat plates set at 90^{o} to one another with a common leading edge (Figures 14 and 15). Boundary layers grew from the common leading edge. The leading edge was given an approximately elliptical shape which extended back one inch.

The model was made from ¼ inch thick plexiglas and aluminum. Both materials were used in the as-delivered state and the surfaces were not ground. The model is 9.75 inches wide by 48 inches long. Forty-six pressure measuring orifices (0.040 inch inside diameter) were placed in the aluminum side (Figure 18).

The model was placed in the center of the water tunnel (Figures 16 and 17). By measuring the surface pressure distribution and moving the model using the linear motion feedthroughs on the bottom of the test section the model could be aligned so that there was no streamwise pressure gradient ($C_p < 0.03$). This alignment was important because the flow would separate with only a slight adverse axial pressure gradient.

The hydrogen bubble generator wire was supported upstream and above the corner, as shown in Figure 15. Various planes could be visualized by moving the height of the wire above the corner.

At a free stream speed of 1/3 ft./sec., the boundary layer on a 48 inch long flat plate is about 0.7 inches. Therefore, the model has a minimum lateral extent of about 14 boundary layer thicknesses. This is sufficient to eliminate edge effects (Ref. 36).

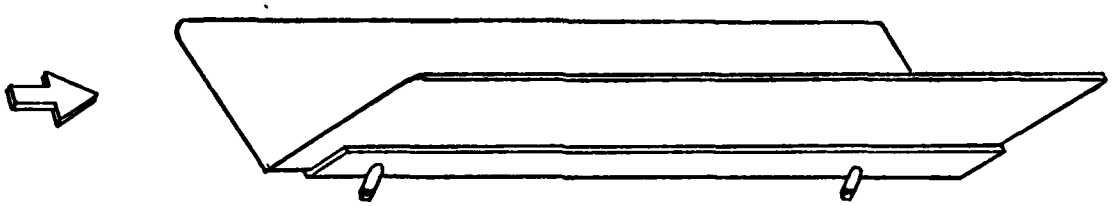

a) Isometric View

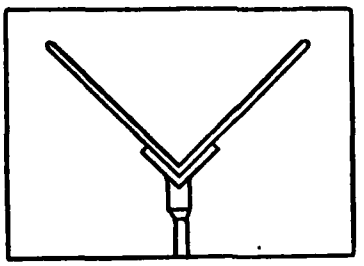

b) End View Mounted in Tunnel

FIGURE 14 Corner Flow Model

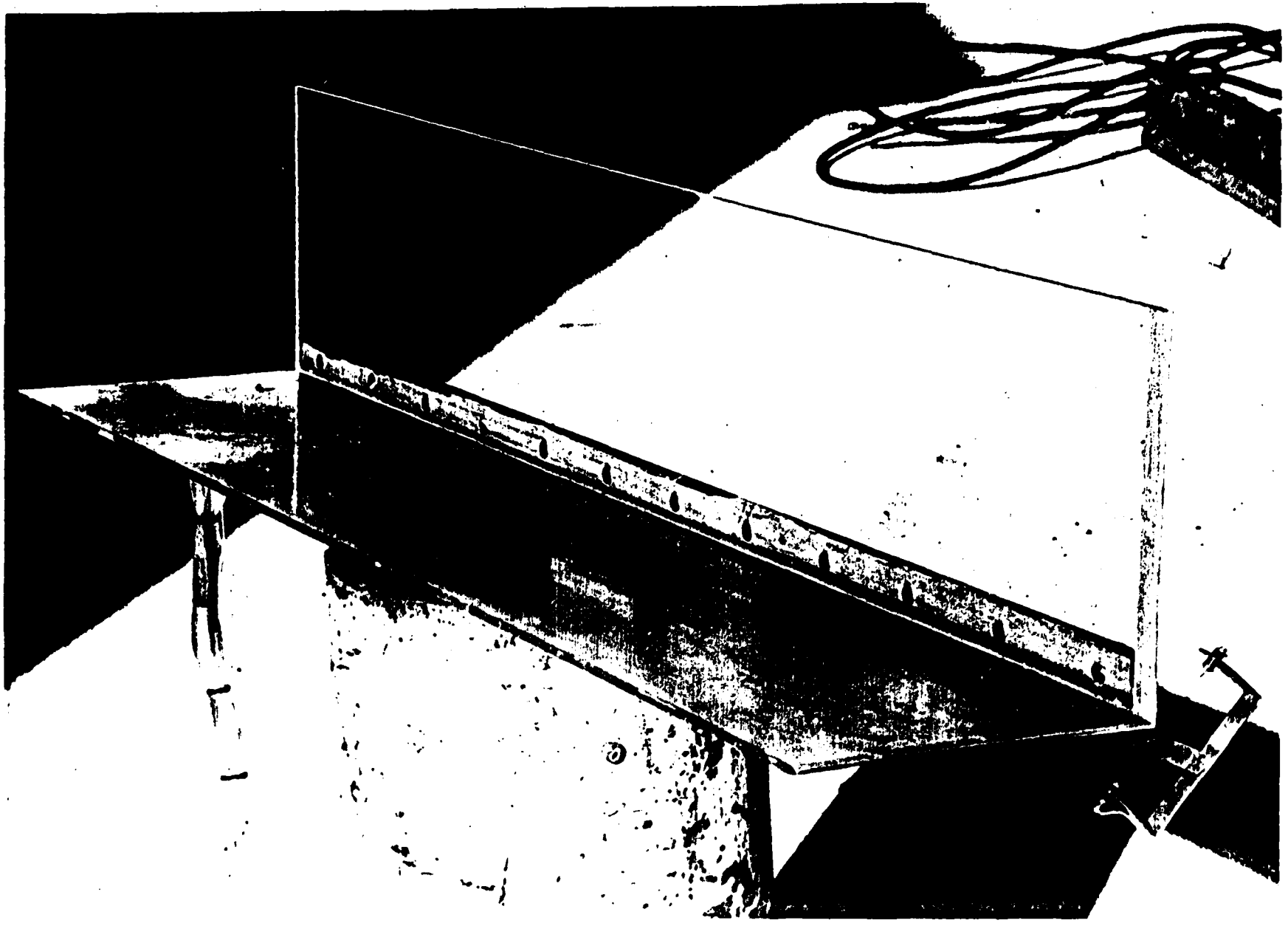

Figure 15 Corner Flow Model with Wire Support

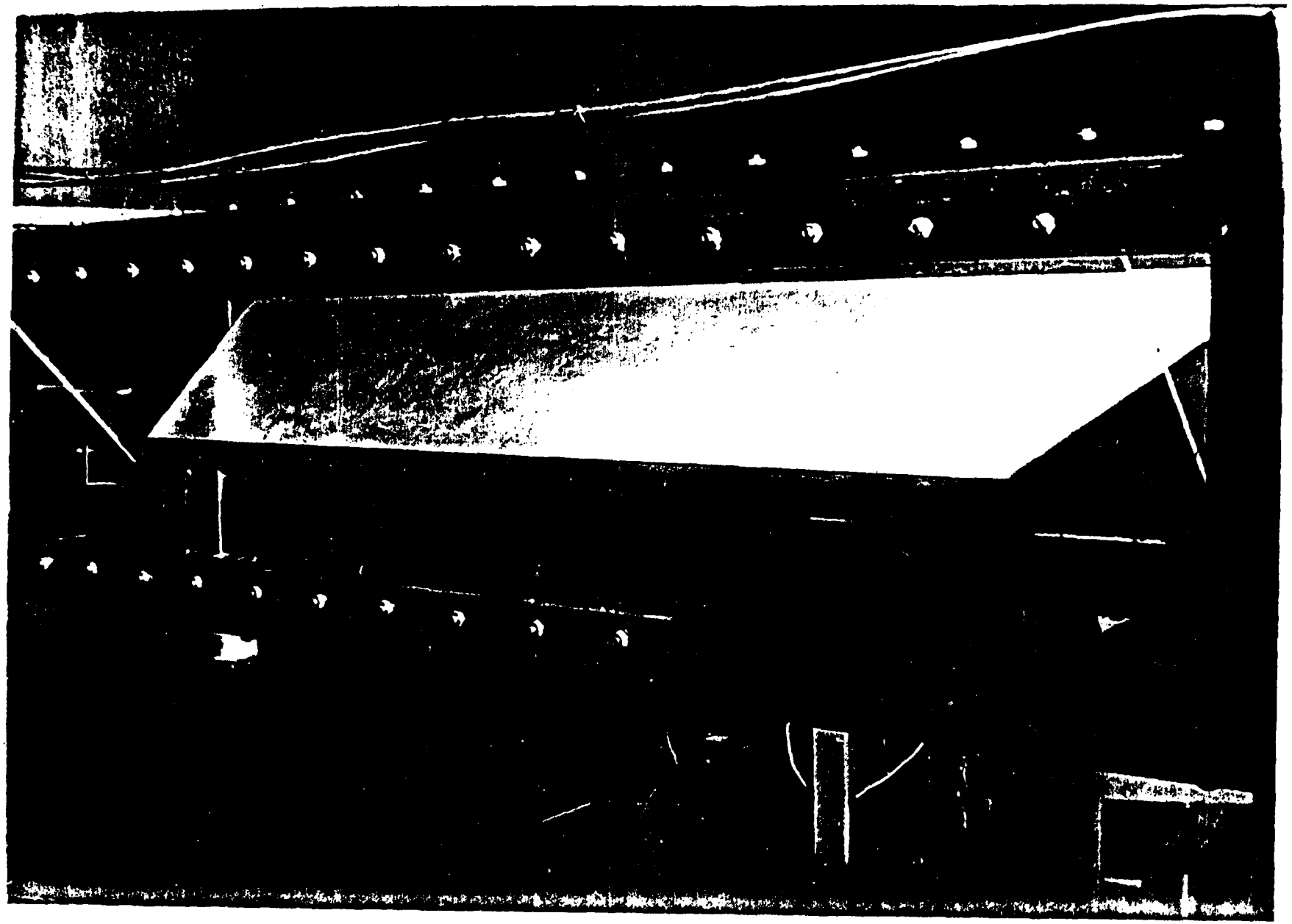

Figure 16 Model Installed in Test Section

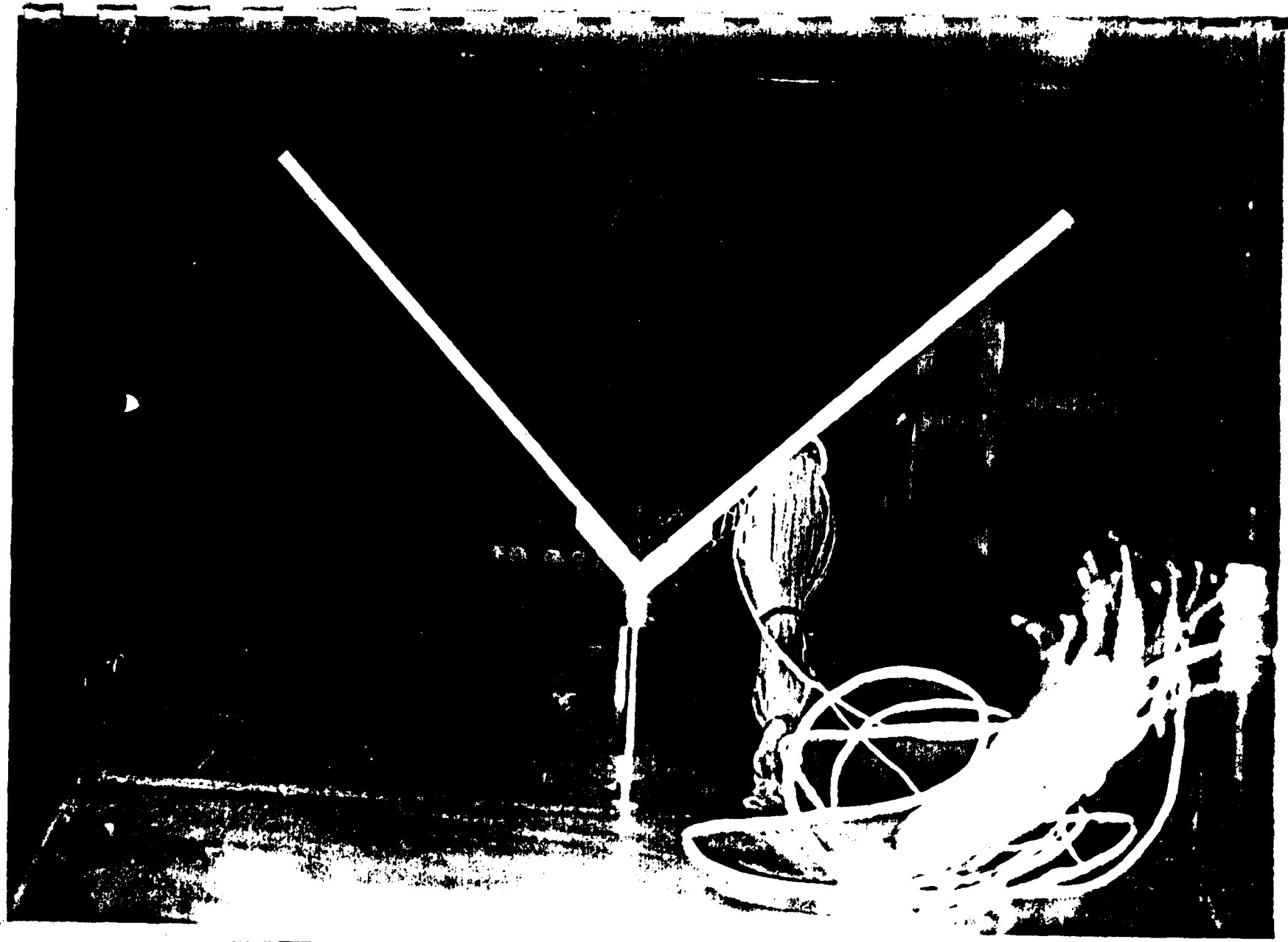

Figure 17 End View of Model in Test Section

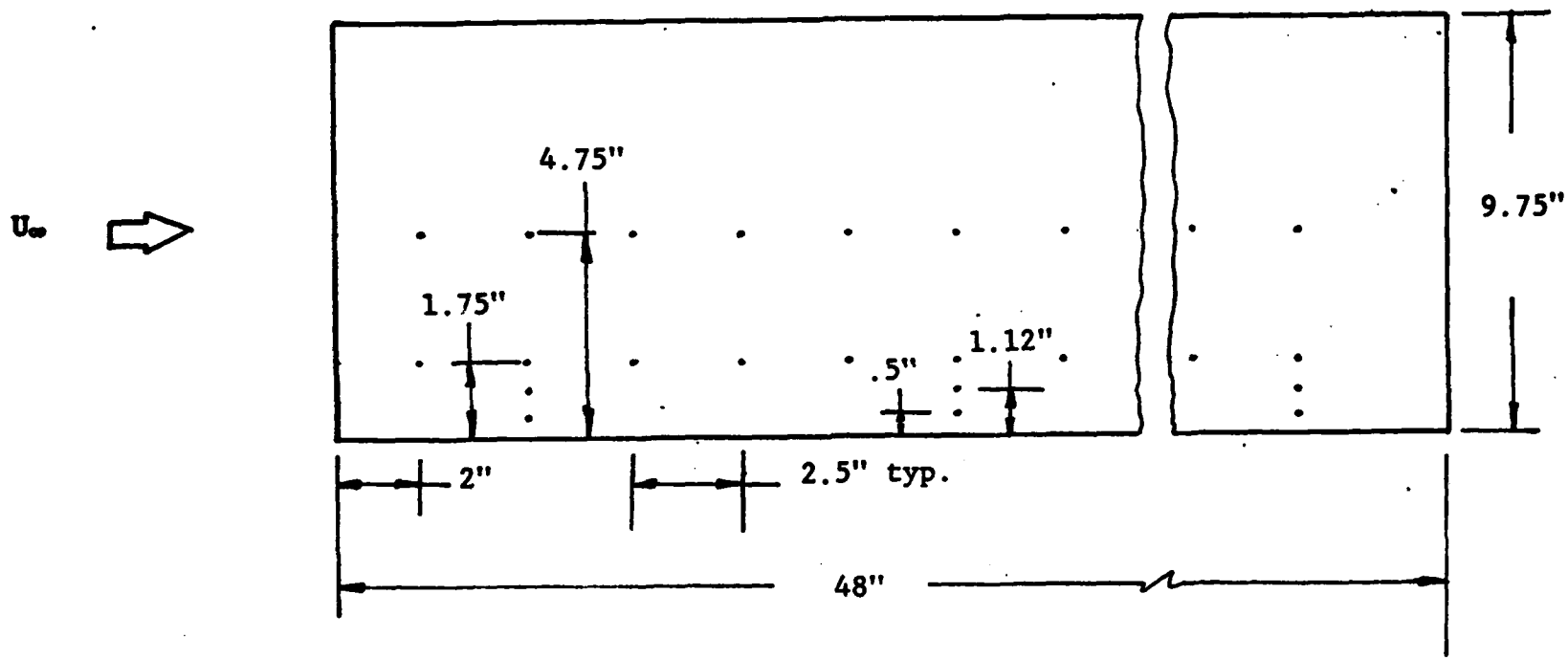

FIGURE 18 Location of Pressure Measuring Orifices

V. RESULTS

The experiments were performed at free stream velocities of approximately 1.7, 3.0, and 8.0 inches/sec. These speeds corresponded, roughly (depending upon the water temperature) to Reynolds numbers per foot of 1.1, 2.0, and 5.25×10^4, respectively. Zamir (Ref. 19) found that transition occurred at a length Reynolds number of 6×10^4 which meant that the flow was laminar over the entire model length at the lowest speed but transitioned after 36 inches and 14 inches, respectively, for the higher speeds. The free stream velocity was measured by timing the travel of some hydrogen bubbles.

Initially the hydrogen bubbles were generated from a 0.001" diameter platinum wire. However, the sheet of bubbles proved to be too difficult to illuminate in the corner of the model and the wire was replaced by a .0045" diameter monel wire that was corregated (10 corregations per inch) by passing it through a pair of gears. The bubbles generated by the wire then came together and were released at the downstream peaks of the corregations forming streaklines from these points (see Figure 19). The streaklines were easier to photograph because of the increased number of bubbles and because the bubbles were larger (the bubble diameters are approximately equal to the diameter of the wire - see Ref. 37). The hydrogen bubbles were generated with 70 volts between the wire and the model and about 200 ma of current flowed between the electrodes. The wire was

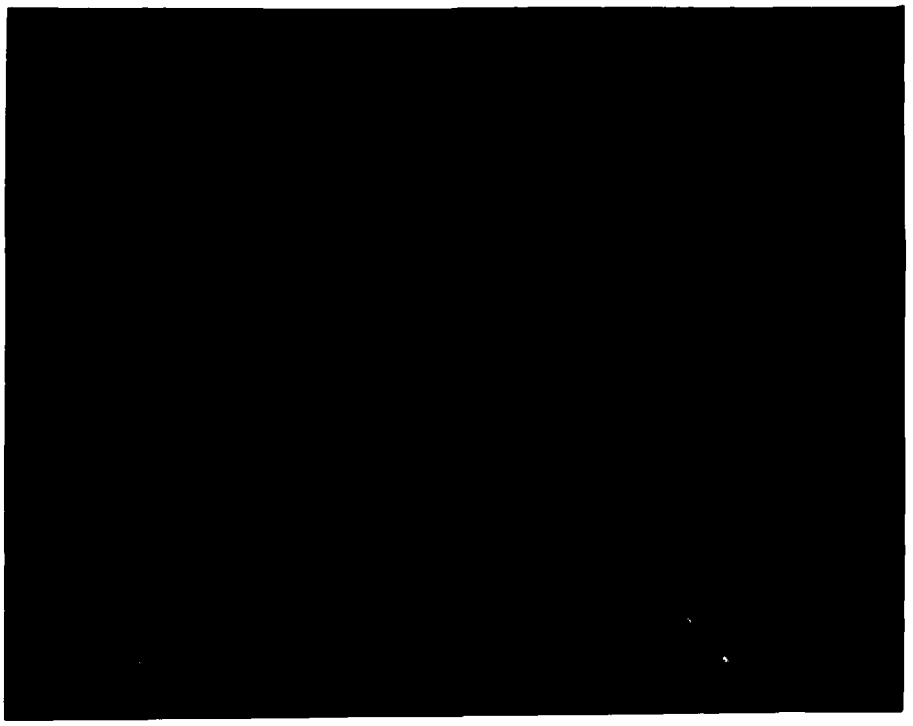

FIGURE 19. HYDROGEN BUBBLE GENERATION

FIGURE 20. DYE INJECTION

placed 0.6 inches upstream of the model and at two locations, 0.33 and 0.45 inches, above the corner in a plane perpendicular to the bisector of the corner.

There were several problems with the hydrogen bubble flow visualization as applied to the corner flow model. The bubbles were difficult to see against the model and so the aluminum plate and a strip in the corner along the plexiglas plate were painted with flat black paint. Then the bubbles were illuminated from the side with a quartz lamp and photographed from above. However, it was difficult to get sufficient light in the blackened corner to adequately illuminate the bubbles.

The hydrogen in the bubbles is reabsorbed in about three seconds (Ref. 37) and, therefore, even at the highest speed the bubbles could only be seen for about 18 inches along the corner. That should have been sufficient, however, to observe the corner vortices in that case because transition was expected to occur 14 inches from the leading edge of the model. The quality of the bubbles deteriated with time as deposits formed on the wire. Reversing the polarity only partially corrected this problem.

Dye streaks were also used to examine the corner flow. The dye, consisting of a mixture of milk, alcohol, and food coloring (Ref. 38), was emmitted from a hyperdermic needle (0.016" I.D., 0.028" O.D.) that was positioned 1.34 inches upstream of the model (Figure 20). The dye streak was

located approximately as shown is the following diagram. The dye was fed by gravitational head which was varied to

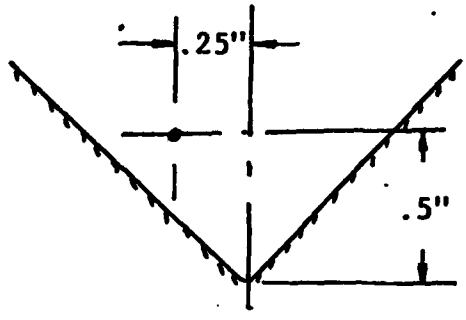

insure that the dye was emitted at a speed close to the water speed so that the streak did not become unstable. The dye streak could be seen for about two feet and then was lost due to diffusion. Dye was also ejected from the first downstream hole that was 0.5" from the centerline (Fig. 18).

Typical results from the hydrogen bubbles and dye are shown in Figures 21 and 22. These photographs show the streaklines only close to the model leading edge because, although they could be seen much further downstream they proved to be difficult to illuminate well enough to photograph. None of the streaklines examined with either the hydrogen bubbles or the dye showed any indication of the presence of secondary motion in the first 18 inches of the corner. This does not conclusively prove that secondary motion does not exist because it is possible that either it exists at other distances from the corner than those

FIGURE 21. HYDROGEN BUBBLE STREAKLINES IN PLANE ABOVE CORNER, 8 IN./SEC.

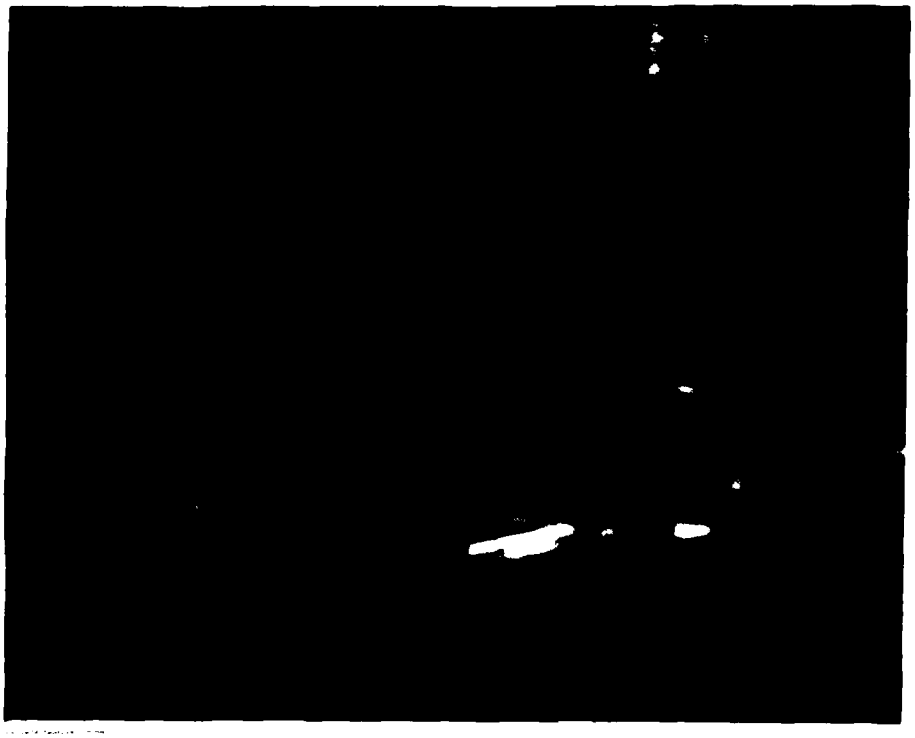

FIGURE 22. DYE STREAKLINE, 1.7 IN./SEC.

examined or that it is poorly developed within the first 18 inches. However, Zamir (Ref. 19) found that the flow became turbulent before the end of that distance for the conditions shown in Figure 21 but the bubbles were absorbed without giving any indication of turbulence in the present experiments. Zamir's evidence for the existence of the secondary motion in a corner was indirect, coming from hotwire velocity profile measurements. He wrote "I was very pleased to hear of your plan to do flow visualization of the corner boundary layer. I recall attempting to do some myself many years ago but without success" (Ref. 15). Therefore, it appears that the secondary motion is very difficult to observe primarily because the visualization seeding material must remain observable for several feet.

Zamir also performed some surface flow visualization which indicated that the flow was toward the corner for laminar flow and away from the corner for turbulent flow (Fig. 3). This result was examined by ejecting dye slowly from the first downstream hole that was 0.5" from the corner, with a freestream speed of 1.7 inches/sec. The dye moved toward the corner while moving only slightly downstream and then became stagnated in the corner. The movement toward the corner is felt to confirm the results of Zamir.

VI. RECOMMENDATIONS

This work has not settled the question of the existence of secondary motion in laminar corner. It was discovered that the common flow visualization techniques that have been developed for water flows were not entirely adequate because of the concavity and size of the present model. Also, there was not enough time to fully explore the corner region with the present techniques and the hydrogen bubble and dye streaks were placed at only several locations relative to the corner. Therefore, more experiments of the present type would be completely justified.

Zamir (Ref. 19) performed all of his experiments with a hot wire which is insensitive to the flow direction. It would be very desirable to repeat his measurements using a two-component (or even three-component) laser velocimeter. Such experiments could be performed more easily in water than in air because of the reduced velocities.

The boundary layer grows simultaneously on both walls for the present model. However, the wing-fuselage junction is more closely modeled by placing a plane on the wall of the tunnel where a boundary layer has already grown (Fig. 23). Measurements of the flow properties, including secondary motions, of this flow and modifications to it (e.g. with transverse curvature in corner) will help in predicting aircraft drag due to interferring surfaces.

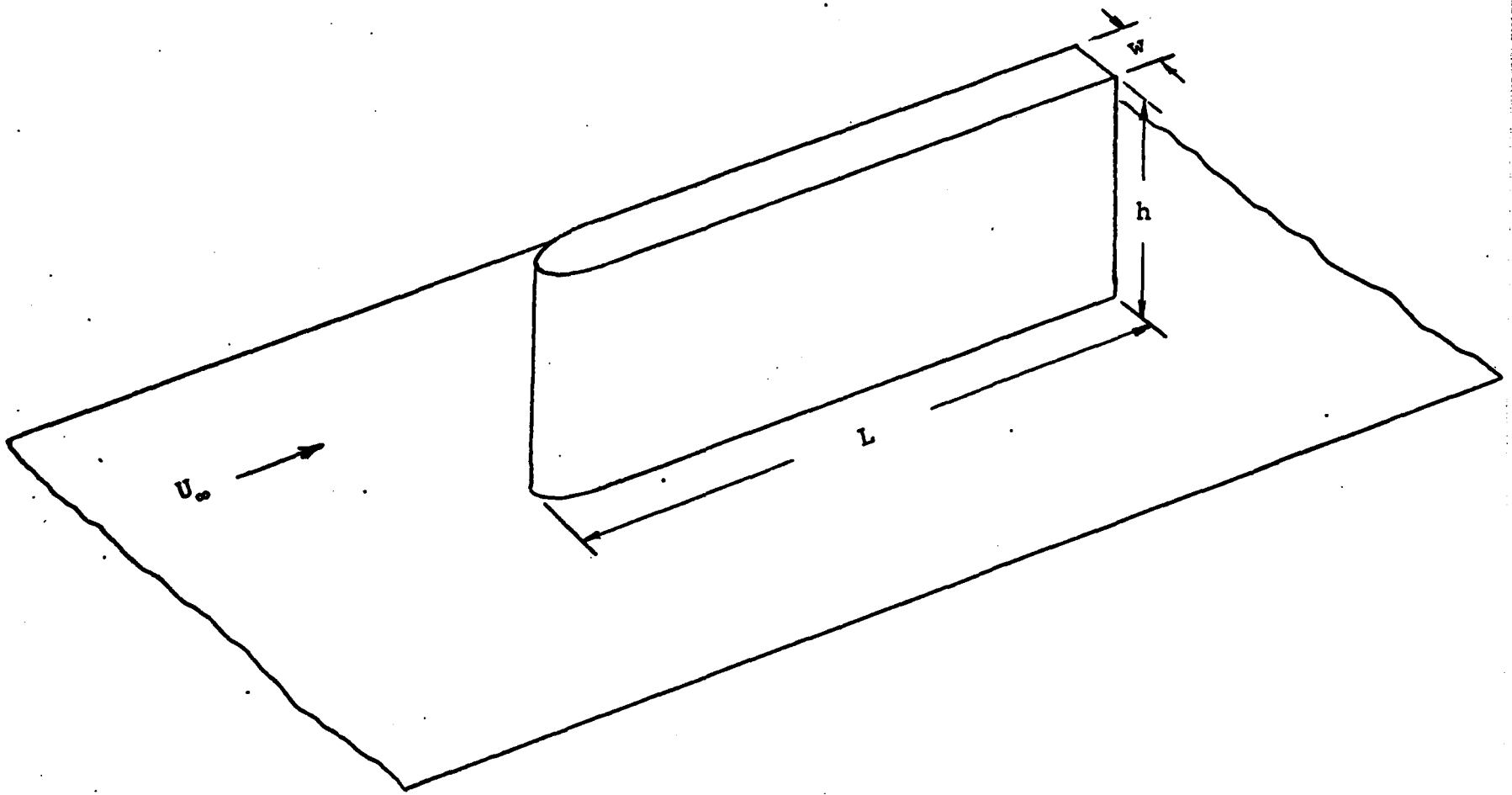

Figure 23. Wing-Fuselage Junction Model

REFERENCES

1. A. M. Lovelace, "Status of Aeronautical Technology," State of the Nation's Air Transportation System, National Academy of Engineering, Washington, D.C., 1976.
2. G. M. Bowes, "Aircraft Lift and Drag Prediction and Measurement," Prediction Methods for Aircraft Aerodynamic Characteristics, AGARD-LS-67, Ref. 4, May 1974.
3. S. F. J. Butler, "Aircraft Drag Prediction for Project Appraisal and Performance Estimation," AGARD Conference on Aerodynamic Drag, AGARD-CP-124, Ref. 6, October, 1973.
4. D. A. Norton, "Airplane Drag Prediction," N. Y. Academy Science Annals 154, 306 (1968).
5. J. H. Paterson, D. G. MacWilkinson, and W. T. Blackerby, "A Survey of Drag Prediction Techniques Applicable to Subsonic and Transonic Aircraft Design," AGARD Conference on Aerodynamic Drag, AGARD-CP-124, Ref. 1, October 1973.
6. A. M. O. Smith and T. Cebeci, "Remarks on Methods for Predicting Viscous Drag," AGARD Conference on Aerodynamic Drag, AGARD-CP-124, Ref. 7, October 1973.
7. R. H. Korkegi, "Survey of Viscous Interactions Associated with High Mach Number Flight," AIAA J. 9, 771 (1971).
8. T. Weeks, "Reynolds Number, Separation, and Intelligent Wall Work at AFFDL," Presentation for AFOSR Summer Study Design Program, UTSI, 1977.
9. R. E. Dix, "Evaluation of an Internal Balance - Supporting Bracket Simulating Lug Suspension for Captive Stores in Wind Tunnel Tests," AEDC-TR-76-117, 1976.

10. J. H. Paterson, "Evolution of Theoretical Aerodynamic Methods and Wind Tunnel Testing at the Lockheed-Georgia Company," Presentation for AFOSR Summer Study Design Program, UTSI, 1977.

11. J. R. Hagerman, Private Communication, August 1977.

12. B. W. Marschner, R. L. Young, and others, "Integration of Wind Tunnels and Computers," USAF/ASEE Fellowship in Engineering Systems Design, AEDC & UTSI, June-August 1977.

13. J. G. Marvin, "Experimental Requirements for NASA's Program in Turbulence Modeling," NASA Ames Research Center.

14. J. G. Marvin, "Experiments Planned Specifically for Developing Turbulence Models in Computations of Flow Fields Around Aerodynamic Shapes," AGARD Conference on Numerical Methods and Windtunnel Testing, AGARD-CP-210, Ref. 14, October, 1976.

15. M. Zamir, Private Communication, December 21, 1978.

16. J. P. Johnston, "Internal Flows," Turbulence, P: Bradshaw, editor, Springer-Verlag, New York, 1976.

17. T. Cebeci and P. Bradshaw, Momentum Transfer in Boundary Layers, McGraw-Hill, New York, 1977.

18. L. Rosenhead, Editor, Laminar Boundary Layers, Oxford University Press, Oxford, England, 1963.

19. M. Zamir and A. D. Young, "Experimental Investigation of the Boundary Layer in a Streamwise Corner," Aero. Quart. 21, 313 (1970).

20. G. M. Bragg, "The Turbulent Boundary Layer in a Corner," J. Fluid Mech. 36, 485 (1969).

21. F. B. Gessner and J. B. Jones, "A Preliminary Study of Turbulence Characteristics of Flow Along a Corner," Tran. ASME, J. Basic Eng., p. 657 (1961).

22. F. B. Gessner and J. B. Jones "On Some Aspects of Fully-Developed Turbulent Flow in Rectangular Channels," J. Fluid Mech. 23, 689 (1965).

23. I. M. M. A. Shabaka, "A Preliminary Experimental Investigation of Turbulent Flow in a Simplified Wing-Body Junction," IC-Aero-75-05, July 1975.

24. H. H. Fernholz, "External Flows", Turbulence, P. Bradshaw, editor, Springer-Verlag, New York, 1976.

25. W. H. Heiser, Presentation for AFOSR Summer Study Design Program, UTSI, 1977.

26. H. Schlichting, Boundary Layer Theory, 6th Ed., McGraw-Hill, New York, 1968.

27. G. F. Carrier, "The Boundary Layer in a Corner," Quart. Appl. Math 4, 367 (1964).

28. F. K. Moore, "Three Dimensional Boundary Layer Theory," in Advances in Applied Mechanics, Volume IV, pp. 159-228, Academic Press, 1956.

29. A. Mager, "Three-Dimensional Laminar Boundary Layers," High Speed Aerodynamics and Jet Propulsion, Volume IV, pp. 286-394, Princeton University Press, 1964.

30. S. G. Rubin, "Incompressible Flow Along a Corner," J. Fluid Mech. 26, 97 (1966).

31. S. G. Rubin and B. Grossman, "Viscous Flow Along a Corner: Numerical Solution of the Corner Layer Equations," Quart. Appl. Math. 29, 169 (1971).

32. N. Tokuda, "Viscous Flow Near a Corner in Three Dimensions," J. Fluid Mech. 53, 129 (1972).

33. K. N. Ghia, "Three-Dimensional Boundary-Region Flows," Lecture Notes Prepared for Short Course on Advances in Computational Fluid Dynamics, UTSI, December 9-13, 1974.

34. K. N. Ghia and R. T. Davis, "A Study of Compressible Potential and Asymptotic Viscous Flows for Corner Region," AIAA J. 12, 355 (1974).

35. R. I. Loehrke and H. M. Nagib, "Control of Free Stream Turbulence by Means of Honeycombs: A Balance Between Suppression and Generation", J. Fluids Eng. 98, 342 (1976).

36. E. B. Davies and A. D. Young, "Streamwise Edge Effects in the Turbulent Boundary Layer on a Flat Plate of Finite Aspect Ratio," ARC R&M No. 3367, 1964.

37. F. A. Schraub, S. J. Kline, J. Henry, P. W. Runstadler, Jr., and A. Littell, "Use of Hydrogen Bubbles for Quantitative Determination of Time-Dependent Fields in Low-Speed Water Flows", J. Basic Eng., Trans. ASME, Series D, 87, 429-444 (1965).

38. H. Werlé, "Hydrodynamic Flow Visualization", Ann. Rev. Fluid Mech. 5, 361-382 (1973).